

Model of motility by spatiotemporal modulation of active interactions

Dominik Schildknecht* and Matt Thomson†

Division of Biology and Biological Engineering, California Institute of Technology, Pasadena, California 91125, USA

(Dated: June 7, 2022)

Transport at microscopic length scales is essential for various technologies and in biological systems. Recent experiments applied spatiotemporal control of active matter to achieve self-organized transport in microtubule-based active matter. Here, this experimental motility mechanism is analyzed with a novel particle-based model. The analytic treatment of the model reveals the fundamental mechanisms for material transport, and simulations demonstrate the model’s extensibility, enabling the simulation of future designs of improved transport protocols in light-controlled active matter devices.

Transport at the micron length scale is essential for technologies such as microfluidics [1, 2] and in biological systems such as in cell motility [3, 4] and intracellular processes [5–7]. While in most technical applications, transport arises as the response of a system to externally applied forces, biological systems rely on self-organization to achieve material transport. Because the biological systems are intrinsically out of equilibrium, transport can not be explained by linear response theory [8]. This property makes these systems fascinating to study, but also much more challenging to understand. Indeed, there have been various *in vivo* and *in vitro* studies trying to address biological transport phenomena at the micron length scales. However, they remained challenging due to the non-linear, self-organized nature of transport and the “molecular complexity” in biological systems [3–7].

In order to understand the physics of biological systems in more detail, so-called active matter was introduced, which refers to systems that continuously transform energy to power various intrinsic processes such as self-propulsion or binding and unbinding of chemical links (see, e. g., Ref. [9] for a review). One area of active matter research focuses on the behavior of different classes of active Brownian particles [10–14]. These systems have been examined, for example, to understand phenomena such as the emergent phase separation arising from repulsive interactions [15–17]. More recently, spatiotemporal modulation of the single-particle velocity (representing the activity in these systems) was introduced [18–21], enabling the construction of microfluidic devices through self-assembly [22].

In general, particle-based active-matter systems focus on the emergent dynamics of individual agents, modeling the dynamics of interacting populations of molecules, cells or organisms. In this area, active Brownian particles are successful in describing the emergent phenomena, even though their interactions are predominantly repulsive [17]. However, since the interactions are mostly repulsive, their self-organization capability is limited, and the necessary structures for material transport and motility in intracellular processes are challenging to assemble. Such processes have been examined

by protein-based active matter, consisting of a contractile network, experimentally realized by a mixture of microtubules and kinesin [23–25]. Using these protein-based active-matter systems, one can systematically analyze how self-organization can lead to structures such as vortices and asters. Furthermore, the complex organizational behavior observed in these systems inspired interesting modeling approaches that rely on a hybrid between hydrodynamics and active nematicity [26–29]. Self-organization phenomena occurred both in experiments and models [24, 25, 30, 31], but because the chemical reactions happen everywhere, they are challenging to isolate and inspect in detail. To focus on the relevant mechanisms, localization of the chemical reactions is imperative. The required localization was recently achieved by introducing light-activated reversible linking between the kinesin motors, leading to a spatially confined contraction of the microtubule network [32]. The excellent spatial control of the contractile microtubule network was then used to demonstrate the directed motion of asters for the first time. While the experiments provided some insights into the physics of contractile networks and material transport in these systems, they require a theoretical model to interpret the results.

In this letter, such a model of material transport in spatiotemporal-activated contractile networks is introduced by a particle-based description in analogy with the Vicsek model of flocking [33]. An elementary description of agents and their mutual interactions can provide insights into the influence of microscopic parameters. Specifically, the model introduced here has a simple limit, which reveals that the fundamental mechanism of transport can be understood in terms of the conservation of momentum, and more precisely, by the conservation of the center of mass in systems with vanishing total momentum. Specifically, we show that spatiotemporal localization of particle interactions can generate directed and organized transport.

Then, simulations are used to validate our results for the intrinsic limitations on transport in the simple model and to understand an extended model with additional features of microtubule-kinesin systems, such as retained activation and hydrodynamic interactions, which can sta-

bilize the mass transport.

Here, we propose a coarse-grained model of the experimental system that collects small clusters of microtubules and motors into N point-like particles in two-dimensions, which neglects the sub-structure of each cluster [34]. The particles can either be active or inactive, described by $p_j = 1$ or $p_j = 0$, respectively. Only active particles interact directly so that one time-step is

$$\vec{x}_i(t + \Delta t) = \vec{x}_i(t) + \Delta t \vec{v}_i(t), \quad (1a)$$

$$\vec{v}_i(t + \Delta t) = \frac{\Delta t}{m_i} \left(\vec{F}_i^{(a)}[\{\vec{x}_j\}_j] + \vec{F}_i^{(f)}[\{\vec{x}_j\}_j] \right), \quad (1b)$$

$$\vec{F}_i^{(a)}[\{\vec{x}_j\}_j] = -\nabla_i \left[\frac{k}{2} \sum_{i \neq j} p_i p_j (\vec{x}_i - \vec{x}_j)^2 \right], \quad (1c)$$

$$\vec{F}_i^{(f)}[\{\vec{x}_j\}_j] = 6\pi\mu\xi_I \vec{u}_i. \quad (1d)$$

In these equations, the momentum term $\vec{v}_i(t)$ is excluded from Eq. (1b), assuming that the drag is highly efficient in dissipating the kinetic energy. Explicit treatment of the drag could be included, however, requiring a considerably smaller time step. It should be noted, that a mathematically equivalent formulation arises for particles with a friction term $-\gamma_i \vec{v}_i$ in the limit of vanishing mass. Then, $\Delta t/m_i$ in Eq. (1b) should be replaced by γ_i^{-1} .

In this model, two forces are introduced: The active force $\vec{F}^{(a)}$ is derived from a spring potential with spring constant k , describing the active interactions in agreement with the experiment, which observed a linear relationship between aster separation and their terminal velocity [32]. Here, no explicit upper bound on the interaction range is enforced, since the localized activation naturally provides a truncation. The second force $\vec{F}^{(f)}$ describes the hydrodynamic interactions between all particles. In this model, μ denotes the viscosity, and $\vec{u}_f(\vec{x}_i; \{\vec{x}_j\}_j, \{\vec{v}_j\}_j)$ is the fluid velocity at point \vec{x}_i generated by the other particles. The fluid velocity is derived by assuming that each particle generates a two-dimensional Stokeslet flow field [35] proportional to its velocity,

$$\vec{u}_i = \frac{\xi_{II}}{4\pi\mu} \sum_{i \neq j} \left(\frac{\vec{v}_j \cdot \vec{x}_{ij}}{|\vec{x}_{ij}|^2} \vec{x}_{ij} - \vec{v}_j \log |\vec{x}_{ij}| \right), \quad (2)$$

where $\vec{x}_{ij} = \vec{x}_i - \vec{x}_j$. In our model, two parameters control the strength of the hydrodynamic interactions, namely ξ_I in Eq. (1d) and ξ_{II} in Eq. (2), which are combined into the single fluid-particle coupling constant $\xi = \xi_I \xi_{II}$.

Furthermore, spatiotemporal control of activity is introduced in the following way: A particle j becomes active at time t if $\vec{x}_j \in \mathcal{A}(t)$, where $\mathcal{A}(t)$ describes the activation area due to the external stimulus, such as the light-activation pattern in the experimental system [32]. In the most elementary version of the model, a particle will deactivate immediately after leaving \mathcal{A} . However,

later in this letter, the influence of retained activity will be analyzed. There, the deactivation is not immediate but is instead governed by a Poisson point process, leading to an exponential decay of the activation probability with activation decay rate λ . The elementary model is retrieved for $\lambda \rightarrow \infty$ so that the “memory” of each particle becomes infinitely short, and they indeed deactivate immediately after they leave \mathcal{A} . In this letter, the discussion is restricted on the experimentally analyzed situation [32], of \mathcal{A} being a circle with radius r moving in a straight line with velocity v .

For the numerical integration of the model, the following (non-dimensional) values are used if not specified differently: The system consists of 4960 particles in a square-shaped box with area 4². The box is co-moving with the activation area with radius $r = 0.5$, and particles are added and removed from the simulation to keep a constant density of 310 particles per unit area in the (non-activated) area that appears newly to the co-moving box. This system is integrated for 1000 time steps with $\Delta t = 0.01$. The mass of each particle and the spring constant are $m_i = k = 1$ for simplicity (leading to $\gamma_i = 100$ in the formulation of Eq. (1b) in terms of friction). For now, $\xi = 0$ and $\lambda \rightarrow \infty$ so that the hydrodynamic interactions and the activation retention can be ignored.

The typical time evolution of such a system is presented in Fig. 1 for the first 500 time steps. Specifically, the time dependence of the mass of activated particles m_a is shown, annotated with illustrations of the configurations. At the beginning of the simulation, the mass inside the initial circle $\mathcal{A}(t = 0)$ is activated, which contracts to form a massive core, as can be observed in the inset (a) of Fig. 1. In analogy with experiments [32], the massive core will be referred to as an aster. Subsequently, material in front of the aster is newly activated, fusing with the aster leading to an increase in m_a and an effective mass transport by shifting the center of mass [cf. inset (b) in Fig. 1]. This process is sustained until the aster becomes too massive to be moved by the newly activated material. Finally, the aster leaves the activation area and breaks apart, as seen in the inset (c) in Fig. 1, which leads to a rapid drop in activated mass.

As demonstrated in the remainder of the paper, such breakup events occur for various values of system parameters. However, the time at which they occur can vary strongly. To quantify the breakup behavior, the time until the first significant drop in activated mass is considered. Intuitively, the longer it takes until the rapid drop occurs, the more stable is the mass transport. Here, the breakup time τ_b is defined as the first time that the activated mass m_a decreases significantly. Formally,

$$\tau_b = \min_{t > 0} \left\{ t \left| \frac{d}{dt} \bar{m}_a(t) < 0 \right. \right\}, \quad (3)$$

where \bar{m}_a is the (centered) moving average of m_a . The moving average is required due to fluctuations arising in

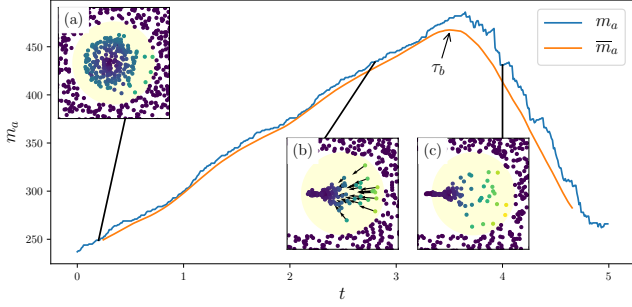


FIG. 1. Time evolution of the activated mass $m_a(t)$ and its moving average $\bar{m}_a(t)$ for a system with $v = 0.2$. The curve is annotated with illustrations of the configurations: The particles are color-coded according to their velocity where violet indicates standing still, blue moving slow and yellow moving fast. The activation region is highlighted in faint yellow. Finally, inset (b) additionally depicts the particle velocities, illustrating the merging process.

simulations. A window size for the moving average of $t_w = 0.5$ was used, but variation of the window size only affected the results marginally.

For an intuitive understanding of the fundamental mechanisms and the breakup time, the sketch in Fig. 2a can be considered, which illustrates the moving activation pattern. In the limit of very large spring constants, the timescale for contraction is much faster than the timescale associated with moving of the activation pattern. In this limit, the collision of the aster and the newly activated mass sickle is instantaneous so that no activated particle is lost and all activated mass is accumulated at a single point. Because the momentum of the system vanishes, the center of mass remains invariant, and all mass is collected at the center of (activated) mass. For a constant density of particles, the center of mass is at the center of the area that was activated at any time. According to the geometry presented in Fig. 2a, the center of mass's velocity is, therefore, half of the activation area's velocity. Without memory, the breakup occurs immediately once the center of mass leaves the activation area \mathcal{A} , therefore,

$$\tau_b = 2 \frac{r}{v} \quad (4)$$

so that the aster travels exactly $d = 2r$ before breaking apart [36]. For smaller spring constants, the aster will lag behind the center of mass, leading to an earlier breakup. Therefore, the expression in Eq. (4) is an upper limit for the breakup time.

This prediction is indeed validated by the simulation results with finite spring constant presented in Fig. 2b. Here, the curves converge to the theoretical limit for increasing spring constants. Furthermore, all τ_b curves exhibit the inverse proportionality with respect to the velocity, generalizing the prediction of Eq. (4) to finite k .

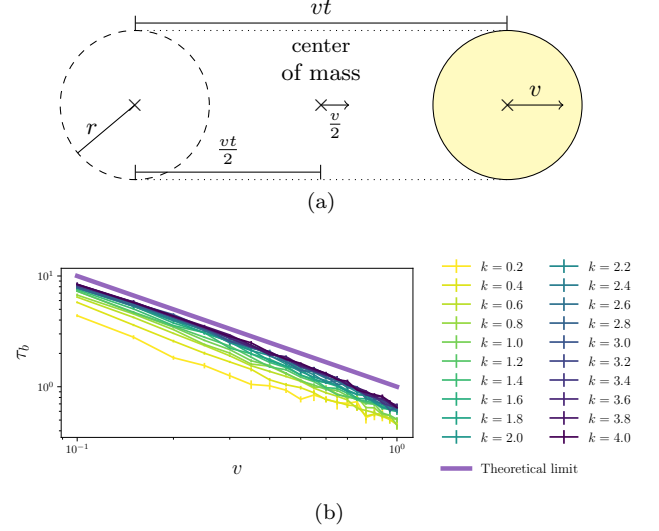
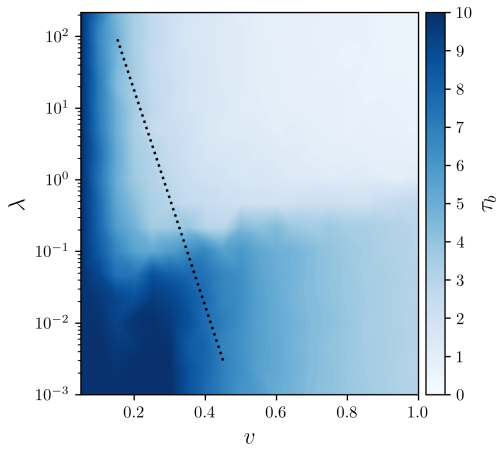


FIG. 2. In Fig. 2a, the analytic calculation is exemplified: The dashed circle indicates the initial activation pattern, the dotted lines the path of the pattern, and the faint yellow circle the activation area at time t . In Fig. 2b, the breakup time τ_b from simulations as a function of activation pattern velocity v for various spring constants k is compared to the theoretical limit. Inverse proportionality can be observed for all k , where the curves for larger k asymptotically approach the theoretical limit given in Eq. (4).

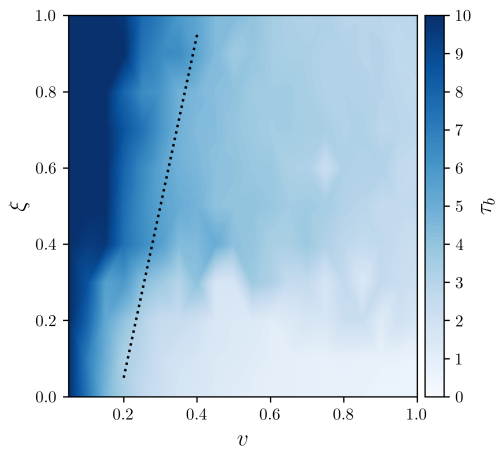
While the simulation results presented in Fig. 2b can be well understood in the theoretical framework, it is not representative of the experiments [32]. Specifically, the aster remains temporarily stable even after it leaves the activation area. Therefore, the disassociation of motors in the microtubule-kinesin system in the experiment is not immediate, and the individual components have some memory of being activated. In our model, retained activation is introduced by deactivating particles in a Poisson point process, which surmounts in a finite (rather than infinite) activation decay rate λ . Therefore, the particles do not deactivate immediately upon leaving the activation area \mathcal{A} , but rather their probability of being active decreases exponentially with time constant λ^{-1} .

Like in Fig. 2b, the breakup time τ_b is considered the measure for the system's stability. Intuitively, we expect that the breakup time is increased for longer memory because the mass is not immediately deactivated, and mass outside of the activation area can be recaptured. Indeed, from the simulation results for $\tau_b(v, \lambda)$ presented in Fig. 3a, it can be observed that the aster becomes more stable for longer memory (smaller λ). Therefore, one possible route for more stable asters lies in increasing the disassociation time of motors.

Moreover, it was shown experimentally that hydrodynamic interactions strongly influence the observed behavior of active matter systems [32, 37]. The rigorous treatment of the hydrodynamic interactions is generally



(a) $\tau_b(v, \lambda)$ for $k = 1$ and $\xi = 0$



(b) $\tau_b(v, \xi)$ for $k = 1$ and $\lambda = \infty$

FIG. 3. Breakup time as a function of two additional parameters, where the dotted lines serve as a guide to the eye. In Fig. 3a, the effect of retained activation is shown, where longer memory (smaller λ) increases τ_b , stabilizing the aster. Similarly, in Fig. 3b, the influence of hydrodynamic interactions is shown. Here, a stronger fluid-particle coupling ξ increases the stability of the aster. It should be noted that the darkest color indicates $\tau_b \geq 10$ as no breakup occurred during our simulations.

challenging and beyond the scope of this letter. However, a simplified treatment using Stokeslets proportional to the single-particle velocities as introduced in Eqs. (1d) and (2) is sufficient to describe some features at least qualitatively. Hence, a finite fluid-coupling parameter ξ is introduced, leading to an effective hydrodynamic interaction between all particles. The simulation data for $\tau_b(v, \xi)$ is presented in Fig. 3b, where larger breakup times can be observed for larger ξ values. This stabilization of the aster arises because the hydrodynamic interactions funnel inactive material from the sides of the activation path into the front of the aster. This process

leads to a higher density of particles in front of the aster, shifting the center of mass further towards the newly activated material, which increases the breakup time and stability. Experimentally, one could exploit this stabilization mechanism by increasing the fluid-particle interaction by some additives or by increasing the material density in front of the aster by priming the path.

In conclusion of this letter, a novel pointlike-particle model for light-activated microtubule-kinesin systems [32, 37] was introduced. The model possesses sufficiently elementary limits to derive analytic results, while at the same time being versatile enough to include complicated effects, such as retained activation or hydrodynamic interactions. It was revealed that the transport arises due to the conservation of the center of mass, which can be shifted by using the spatiotemporal modulation of interactions, leading to a controlled mechanism for motility. Furthermore, the calculation also demonstrates the limitations of the motility due to the mass accumulation, making the transport gradually more difficult.

Additionally, simulations were used to model two features of microtubule-kinesin systems: retained activity and hydrodynamic interactions. The extensions proved to be simple, showcasing the versatility of the model. Both features stabilize the mass transport in the form of an aster for a longer time, but their mechanisms are quite different. Retained activation yields longer interaction times for the system, where hydrodynamic interactions lead to the incorporation of otherwise inactive material and a density increase in front of the aster, increasing the control over the center of mass.

In contrast to the single-particle activation in active Brownian particles [19, 20], the model proposed in this letter can induce directed motility. While the active Brownian particles show exciting applications [22], the interaction-based model is an ideal starting point for systematically analyzing microscopic transport. Due to the versatility of the model, various other features could be analyzed. One could analyze more realistic particle-particle interactions, the finite extent of particles, or more realistic hydrodynamic interactions, for example, by using a lattice Boltzmann approach [38, 39]. Moreover, only circular activation patterns moving at a constant speed in a constant direction were analyzed, inspired by recent experiments [32]. However, various other spatiotemporal activation patterns could be imagined [22, 37], which could lead to exciting light-activated matter systems. Our model could serve as an intuitive guide for designing applications and should enable rapid prototyping of novel ideas.

Our implementation used several scientific libraries [40–43] and is available online [44]. The data presented in the figures is openly available from the Caltech Research Data Repository at [45].

We thank Jerry Wang, Arjuna Subramanian, Dr. Zijie Qu, and Dr. Shahrar Shadkhoo for scientific discussions

and feedback to the manuscript. Furthermore, we acknowledge funding through Packard Foundation (2019-69662) and the Heritage medical research institute.

* dominik.schildknecht@gmail.com

† mthomson@caltech.edu

- [1] J. S. Kuo and D. T. Chiu, *Annual Review of Analytical Chemistry* **4**, 275 (2011).
- [2] N. Convery and N. Gadegaard, *Micro and Nano Engineering* **2**, 76 (2019).
- [3] T. Mitchison and L. Cramer, *Cell* **84**, 371 (1996).
- [4] L. Blanchoin, R. Boujemaa-Paterski, C. Sykes, and J. Plastino, *Physiological Reviews* **94**, 235 (2014).
- [5] N. Hirokawa, Y. Noda, Y. Tanaka, and S. Niwa, *Nature Reviews Molecular Cell Biology* **10**, 682 (2009).
- [6] D. A. Fletcher and R. D. Mullins, *Nature* **463**, 485 (2010).
- [7] C. Appert-Rolland, M. Ebbinghaus, and L. Santen, *Physics Reports* **593**, 1 (2015), arXiv:1507.06166.
- [8] S. Dal Cengio, D. Levis, and I. Pagonabarraga, *Physical Review Letters* **123**, 238003 (2019), arXiv:1907.02560.
- [9] D. Needleman and Z. Dogic, *Nature Reviews Materials* **2** (2017), 10.1038/natrevmats.2017.48.
- [10] J. R. Howse, R. A. L. Jones, A. J. Ryan, T. Gough, R. Vafabakhsh, and R. Golestanian, *Physical Review Letters* **99**, 048102 (2007).
- [11] Y. Hong, N. M. K. Blackman, N. D. Kopp, A. Sen, and D. Velegol, *Physical Review Letters* **99**, 178103 (2007).
- [12] S. Jiang, Q. Chen, M. Tripathy, E. Luijten, K. S. Schweizer, and S. Granick, *Advanced Materials* **22**, 1060 (2010).
- [13] P. Romanczuk, M. Bär, W. Ebeling, B. Lindner, and L. Schimansky-Geier, *The European Physical Journal Special Topics* **202**, 1 (2012).
- [14] M. E. Cates and J. Tailleur, *EPL (Europhysics Letters)* **101**, 20010 (2013), arXiv:1206.1805.
- [15] I. Theurkauff, C. Cottin-Bizonne, J. Palacci, C. Ybert, and L. Bocquet, *Physical Review Letters* **108**, 268303 (2012), arXiv:1202.6264.
- [16] I. Buttinoni, J. Bialké, F. Kümmel, H. Löwen, C. Bechinger, and T. Speck, *Physical Review Letters* **110**, 238301 (2013), arXiv:1305.4185.
- [17] M. E. Cates and J. Tailleur, *Annual Review of Condensed Matter Physics* **6**, 219 (2015).
- [18] J. M. Walter, D. Greenfield, C. Bustamante, and J. Liphardt, *Proceedings of the National Academy of Sciences* **104**, 2408 (2007).
- [19] G. Volpe, I. Buttinoni, D. Vogt, H. J. Kümmerer, and C. Bechinger, *Soft Matter* **7**, 8810 (2011), arXiv:1104.3203.
- [20] I. Buttinoni, G. Volpe, F. Kümmel, G. Volpe, and C. Bechinger, *Journal of Physics Condensed Matter* **24** (2012), 10.1088/0953-8984/24/28/284129, arXiv:1110.2202.
- [21] A. A. Fragkopoulou, J. Vachier, J. Frey, F.-M. L. Menn, M. Wilczek, M. G. Mazza, and O. Bäumchen, (2020), arXiv:2006.01675.
- [22] J. Stenhammar, R. Wittkowski, D. Marenduzzo, and M. E. Cates, *Science Advances* **2**, e1501850 (2016), arXiv:1507.01836.
- [23] R. Urrutia, M. A. McNiven, J. P. Albanesi, D. B. Murphy, and B. Kachar, *Proceedings of the National Academy of Sciences* **88**, 6701 (1991).
- [24] F. J. Nédélec, T. Surrey, A. C. Maggs, and S. Leibler, *Nature* **389**, 305 (1997).
- [25] T. Surrey, F. Nédélec, S. Leibler, and E. Karsenti, *Science* **292**, 1167 (2001).
- [26] D. Marenduzzo, E. Orlandini, and J. M. Yeomans, *Physical Review Letters* **98**, 118102 (2007).
- [27] D. Marenduzzo, E. Orlandini, M. E. Cates, and J. M. Yeomans, *Physical Review E* **76**, 031921 (2007), arXiv:0708.2062.
- [28] L. Giomi, M. C. Marchetti, and T. B. Liverpool, *Physical Review Letters* **101**, 198101 (2008), arXiv:0805.1680.
- [29] L. Giomi, *Physical Review X* **5**, 031003 (2015), arXiv:1409.1555.
- [30] L. Giomi, L. Mahadevan, B. Chakraborty, and M. F. Hagan, *Nonlinearity* **25**, 2245 (2012), arXiv:1110.4338.
- [31] L. Giomi and A. DeSimone, *Physical Review Letters* **112**, 147802 (2014), arXiv:1310.1908.
- [32] T. D. Ross, H. J. Lee, Z. Qu, R. A. Banks, R. Phillips, and M. Thomson, *Nature* **572**, 224 (2019), arXiv:1812.09418.
- [33] T. Vicsek, A. Czirók, E. Ben-Jacob, I. Cohen, and O. Shochet, *Physical Review Letters* **75**, 1226 (1995).
- [34] P. J. Foster, S. Fürthauer, M. J. Shelley, and D. J. Needleman, *eLife* **4**, 1 (2015).
- [35] A. T. Chwang and T. Y. T. Wu, *Journal of Fluid Mechanics* **67**, 787 (1975).
- [36] In Fig. 2a, the aster would have already broken apart.
- [37] Z. Qu, D. Schildknecht, J. Jiang, E. Amaya, S. Shadkhoo, T. Tsou, H. Jin Lee, T. Roeschinger, J. Stellwagen, N. Razin, R. Phillips, D. Van Valen, and M. Thomson, (in preparation).
- [38] A. J. C. Ladd and R. Verberg, *Journal of Statistical Physics* **104**, 1191 (2001).
- [39] Y. Chen, Q. Cai, Z. Xia, M. Wang, and S. Chen, *Physical Review E* **88**, 013303 (2013).
- [40] J. D. Hunter, *Computing in Science & Engineering* **9**, 90 (2007).
- [41] S. K. Lam, A. Pitrou, and S. Seibert, in *Proceedings of the Second Workshop on the LLVM Compiler Infrastructure in HPC - LLVM '15* (ACM Press, New York, New York, USA, 2015) pp. 1–6.
- [42] Dask Development Team, “Dask: Library for dynamic task scheduling,” (2016).
- [43] K. Greff, A. Klein, M. Chovanec, F. Hutter, and J. Schmidhuber, in *{P}roceedings of the 16th {P}ython in {S}cience {C}onference*, edited by K. Huff, D. Lippa, D. Niederhut, and M. Pacer (2017) pp. 49–56.
- [44] Source code available from: <https://github.com/domischi/SpringBox>.
- [45] <http://dx.doi.org/10.22002/D1.1451>.